Temperature-Dependent Rotational Dipole Mobility and Devitrification of Rigid Amorphous Fraction in Unpoled and Poled Biaxially Oriented Poly(vinylidene fluoride)

Guanchun Rui ^{1,#}, Elshad Allahyarov ^{2,4,5,#}, John J. Thomas, ³ Philip L. Taylor ^{2,*}, and Lei Zhu ^{1,*}

- ¹ Department of Macromolecular Science and Engineering, Case Western Reserve University,

 Cleveland, Ohio 44106-7202, United States
- ² Department of Physics, Case Western Reserve University, Cleveland, Ohio 44106-7079, United

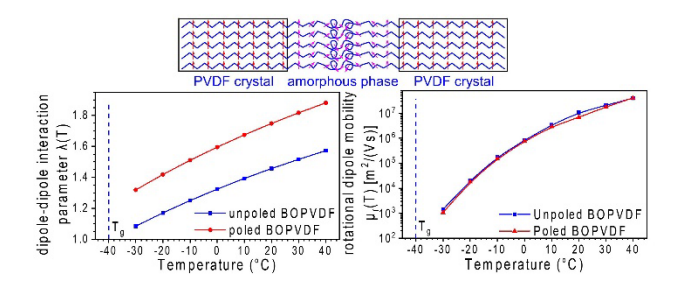
 States
 - ³ Department of Physics and Astronomy, Tufts University, Medford, Massachusetts, 02155, United States
- ⁴ Theoretical Department, Joint Institute for High Temperatures, Russian Academy of Sciences, 13/19 Izhorskaya Street, Moscow 125412, Russia
- ⁵ Institut für Theoretische Physik II: Weiche Materie, Heinrich-Heine-Universität Düsseldorf,

 D-40225 Düsseldorf, Germany

[#] These authors contribute equally to this work.

^{*} Corresponding authors. Emails: lxz121@case.edu (L.Z.) and plt@case.edu (P.L.T.)

Table of Content Graphic



Abstract

In addition to the pronounced ferroelectric property from polar crystalline phases, poly(vinylidene fluoride) (PVDF) and its random copolymers also exhibit high dielectric permittivities as a result of highly mobile dipoles in the amorphous phase. In this study, we developed a new theoretical approach to determine the dipole concentration, dipole moment, dipole-dipole interaction, and rotational dipole mobility for PVDF by means of broadband dielectric spectroscopy. From the permittivity of molten PVDF, the Kirkwood-Fröhlich g-factor and its temperature dependence were determined and used as global parameters for the simulation of unpoled and highly poled biaxially oriented PVDF (BOPVDF). It was found that the concentration of active dipoles substantially increased as the temperature increased from -30 to 40 °C, indicative of the devitrification of the rigid amorphous fraction (RAF). Both the calculated dipole moment and the g-factor of the poled BOPVDF were higher than those of the unpoled BOPVDF, resulting in a higher permittivity and piezoelectric performance. In addition, the dipoledipole interaction was found to increase substantially upon increasing the temperature from -30 to 40 °C, leading to an increase of over 4 orders of magnitude in the rotational dipole mobility. This was direct evidence for the devitrification of RAF in both unpoled and poled BOPVDF.

Introduction

The nature of molecular bonding causes dielectric polymers to exhibit a much lower relative permittivity (usually 2-5) from electronic and atomic polarizations than do ceramics (i.e., ionic crystals), which often have a relative permittivity from a few tens to several thousands. 1, 2 Recently, new electrical applications, such as power electronics in electric vehicles, require miniaturized polymer film capacitors with enhanced permittivities. 3-6 To further increase the dielectric constants for polymers, we have proposed to utilize the orientational polarization, which takes advantage of the rotation of permanent molecular dipoles. 1, 2 For example, water has a high dielectric constant (~80) at room temperature because of the fast orientational polarization from the hydrogen-bonded polar nanoregions, 7 which relax rapidly around 10 GHz. 8, 9 Even after water freezes into ice at 0 °C, the dielectric constant is still high (~90) with the peak relaxation frequency decreasing to ~3 kHz. 10 It is thus highly desirable to achieve water- or ice-like polymers with high dielectric constants and fast orientational polarization without any significant increase of dielectric loss.

Electrostrictive and piezoelectric polymers also require active molecular dipoles with a high rotational mobility. It has been reported that electrostriction of the oriented amorphous fraction (OAF) in ferroelectric polymers, such as poly(vinylidene fluoride) (PVDF) and its random copolymers, is a major source of piezoelectricity. ^{11, 12} In addition, growth of highly mobile relaxor-like secondary crystals in the OAF will further increase the piezoelectric performance. ^{13, 14} For example, high piezoelectric coefficients (d₃₁ and d₃₃) of 60-75 pC/N were achieved for PVDF homopolymer and P(VDF-TrFE) (TrFE is trifluoroethylene) random copolymers with a low VDF content of around 50 mol.%. ^{13, 14, 16, 17} To further enhance the piezoelectric performance of

electroactive polymers, it is thus highly desirable to increase the dipole moments and rotational mobility of the OAF and secondary crystals.

To the best of our knowledge, no thorough investigation of rotational dipole mobility in polar polymers has been reported so far. Here, we combine broadband dielectric spectroscopy (BDS) with a newly developed theoretical approach to determine dipole concentration, dipole moment, dipole-dipole interaction, and dipole rotational mobility for unpoled and highly poled biaxially oriented PVDF (BOPVDF). The goal is to understand their contributions to the high dielectric and piezoelectric properties of PVDF-based electroactive polymers.

Experimental Section

Materials. The BOPVDF film was obtained from Kureha Corporation (Tokyo, Japan) with a uniform thickness of $8.0\pm0.1~\mu m$ (i.e., mean \pm standard deviation). As reported before, ^{12, 18} the crystallinity (x_c) of the unpoled BOPVDF was ca. 0.52, and the crystalline phase contained 70% α and 30% β crystals.

For electric poling, gold (Au) electrodes (ca. 10 nm thick) were coated on both sides of the film sample with an electrode area of 78.5 mm², using a Q300TD sputter coater (Quorum Technologies, Ltd., Laughton, East Sussex, U.K.). High-field unidirectional electric poling was applied at room temperature to transform the 70% α crystals into β crystals, using a Premiere II ferroelectric tester (Radiant Technologies, Inc., Albuquerque, NM) in combination with a Trek 10/10B-HS high-voltage amplifier (0-10 kV AC, Lockport, NY). The poling field was 650 MV/m with a unidirectional sinusoidal waveform (i.e., 325 MV/m DC + 325 MV/m AC) at 1 Hz and room temperature for 100 cycles. After poling, the film contained nearly 100% β crystals. 11, 12 The melt-recrystallized PVDF films were obtained by melting the BOPVDF film at 200 °C, followed

by compression molding. The final film thickness was around 30 µm. All PVDF films were thoroughly dried in vacuum at 50 °C for 2 days and stored in a desiccator before use. To remove impurity ions, the unpoled BOPVDF films were soaked in deionized water for 3 days and thoroughly dried in vacuum at room temperature before electric poling and BDS tests.

Characterization Methods and Instrumentation. A Novocontrol Concept 80 dielectric spectrometer with temperature control (Novocontrol Technologies GmbH & Co., Montabaur, Germany) was used for BDS measurements. The frequency ranged from 1 to 10⁷ Hz and the temperature ranged from -100 to 200 °C. The typical applied voltage was 1.0 V_{rms} (i.e., root-mean square voltage). Au electrodes (78.5 mm²) were sputter-coated on both sides of the film for BDS tests. Temperature-modulated differential scanning calorimetry (TMDSC) was carried out on a Discovery DSC250 (TA Instruments, New Castle, DE). 5.89 mg of melt-recrystallized BOPVDF sample were sealed in an aluminum hermetic pan (47.40 mg), which is almost the same weight (±0.01 mg) as the reference pan. The heating rate was 5 °C/min with a modulation of 0.8 °C in a period of 60 s. The "three-run method" was used to determine the heat capacity of the sample. The first run was an empty pan to obtain the baseline. The second run was sapphire (9.08 mg) to calibrate the heat flow amplitude. The third run was the sample. All the aluminum pans were kept at 47.40±0.03 mg to minimize system errors.

Results and Discussion

Kirkwood-Fröhlich Theory and g-Factor Revisited for Polymers. In the generic BDS experiments, the real part of the relative permittivity exhibits a dielectric relaxation strength, $\Delta \varepsilon_c = \varepsilon_c - \varepsilon_c^0 > 0$, around the angular peak loss frequency ω_d . Here, the high-frequency permittivity ε_c^0 has no contribution from the orientation of molecular dipoles and corresponds to the permittivity

plateau at $\omega \gg \omega_d$. The low-frequency (or static) permittivity, ε_c , contains contributions from the orientational polarization of mobile dipoles and corresponds to the permittivity plateau at $\omega \ll \omega_d$. Several expressions are frequently used to estimate dipolar properties of polymers, utilizing parameters such as the volumetric concentration of dipoles n, the permanent dipole m_d , and the correlation factor g (i.e., the Kirkwood-Fröhlich correlation factor) from the BDS data containing both low- and high-frequency permittivities. These expressions, originally derived for a liquid of polarizable dipoles, are usually rewritten for polar polymers and blends/composites by substituting the low-frequency liquid permittivity $\varepsilon(0)$ by ε_c , the high-frequency liquid permittivity $\varepsilon(\infty)$ by ε_c^0 , and the relative permittivity of vacuum $\varepsilon_v = 1$ by the relative permittivity of the matrix ε_m .

The theoretical background of the g-factor relies on the work by Onsager and Kirkwood. Fröhlich introduced the Kirkwood g-factor, accounting for the local structure and interactions in the dipolar system. All these are well-documented in Kao's book on dielectric solids. ¹⁹ The g-factor values, deduced either from experimental data or simulations, are usually compared with unity in order to determine whether the dipoles tend to align parallel or antiparallel. It is suggested that if g>1, then the dipole-dipole interaction is strong, and any tagged dipole with its neighboring dipoles tend to orient parallel, while g<1 implies a trend for them to orient antiparallel. Although a large amount of effort has been dedicated in attempts to predict g, the deduced g-factors were generally not successful in reproducing the experimentally derived values. Some advances in the calculation of the g factor have recently been reported, ^{20, 21} and an integral formula for the Kirkwood correlation factor has been derived. It was suggested that g>1 does not necessarily mean a strong correlation between the interacting dipoles.

The first expression, known as the Debye extension of the Clausius-Mossotti equation, neglects any intermolecular interactions, and thus is valid only for polar polymers with extremely dilute dipoles having a low permanent dipole moment m_d , ¹⁹

$$\frac{\varepsilon_c - \varepsilon_m}{\varepsilon_c + 2\varepsilon_m} = \frac{n}{3\varepsilon_0} \left(\alpha_{e/a} + \frac{m_d^2 g}{k_B T} \right) \tag{1}$$

where k_B is the Boltzmann constant, T the absolute temperature, ε_0 the vacuum permittivity, and $\alpha_{e/a}$ is the electronic+atomic polarizability of the dipoles. Eqn. (1) demands first-hand knowledge of the molecular polarizability α , and has been shown to provide incorrect values of g and m_d for polar liquids.

The second expression is the classical Kirkwood-Fröhlich theory, 19

$$\frac{(\varepsilon_c - \varepsilon_c^0)(2\varepsilon_c + \varepsilon_c^0)}{\varepsilon_c(\varepsilon_c^0 + 2\varepsilon_m)^2} = \frac{nm_d^2g}{9\varepsilon_0k_BT} = \phi \frac{m_d^2g}{9\varepsilon_0V_dk_BT}$$
(2)

where V_d is the volume of a single dipole, ϕ is the volume fraction of dipoles, and thus $\phi = nV_d$. This equation is considered applicable to molecules having a large permanent dipole moment, and thus to situations where the correlation between a central dipole and the surrounding dipoles cannot be replaced by the response of a continuum dielectric. Eqn. (2) describes the fluctuations of a spherical dipole embedded in a medium having a frequency-independent dielectric constant; however, while this model can provide useful insight by means of computer simulations, it is not widely applicable to real materials. Other modifications of the Kirkwood-Fröhlich theory have also been reported in the literature, 22,23 but their validity remains debatable. In the following, we will use Eqn. (2) to relate the dependence of n, m_d , and g on temperature to the experimental data of $\varepsilon_c(T)$, ε_c^0 , and ε_m by running a fitting procedure to obtain the best match for the left hand side of Eqn. (2).

Theoretical Assumptions for n, m_d , and g-Factor. In the Kirkwood-Fröhlich theory, the experimentally measurable left-hand side of Eqn. (2) is related to a product of the dipole concentration n(T), the square of the dipole moment $m_d(T)$, and the g(T)-factor, all of which are temperature dependent. We thus have one equation and three unknowns, and must make some assumptions about the forms of n(T), $m_d(T)$, and g(T). Experimental results for water and alcohols²⁴ indicate that n(T) and g(T) should have a linear dependence on temperature. We consider two different functional dependencies for $m_d(T)$ on T: a power-law and hyperbolic tangent dependencies. We then have the following relationships:

$$n(T) = n_0 \left(1 + \beta \frac{T - T_0}{T_0} \right) \tag{3}$$

$$g(T) = g_0(1 - \alpha T) \tag{4}$$

$$m_d(T) = m_{d0} \left(\frac{T_0}{T}\right)^{\theta} \tag{5}$$

$$m_d(T) = m_{d0} \left(1 - \tanh \theta \left(\frac{T - T_0}{T_0} \right) \right) \tag{6}$$

where β , α , and θ are fitting parameters. If the sample is initially in a fully molten state at T_0 , then $\beta=0$. However, if the sample consists of both crystalline and amorphous phases at T_0 , then $\beta>0$, i.e., n(T) increases with temperature. We will further discuss the physical meaning of $\beta>0$ for unpoled and poled BOPVDF films later.

Second, the g(T)-factor decreases with T, because thermal fluctuations disrupt orientational correlations between dipoles.^{12, 24} Additionally, we suggest that in PVDF polymers with coexisting amorphous and crystalline phases, the fitting parameters g_0 and α in Eqn. (4) can be used as global parameters for other PVDF samples.

Third, a choice is required for the form of the dipole moment $m_d(T)$. One possibility is, an inverse power-law temperature dependence, as was used by Hodge and Angell for the

permittivity of dipolar fluids.²⁵ According to statistical mechanical theories of dielectrics, the permittivity of a dipolar fluid depends on the fluctuation of the sum of dipole moments of all molecules.²⁶ Therefore, it seems reasonable to assume a power law dependence for the dipole moment of PVDF dipoles in a limited range around room temperature. In amorphous PVDF, the dipole moment of each repeat unit has a positive feedback contribution from the polarization field of neighboring dipoles. For an isotropic state, the additional polarization field is zero on average, which decreases the dipole moment m_{d0} of each repeat unit to the value in a dilute dipolar system. However, arguments could be made for other functional forms, and so to provide an alternative for comparison, we also consider a tanh(x)-based hyperbolic model for the dipole moment.

With the suggested T dependence for n(T), g(T), and $m_d(T)$, there is still uncertainty in the individual magnitudes of n_0 , m_{d0} , and g_0 , as only the product $n \cdot m_d^2 \cdot g$ is experimentally determined. Therefore, to minimize the uncertainty in fitting these constants, it is advisable to know the exact value of at least one of them from the experimental data.

Rotational Self-Diffusion and Fluctuating Dipole Mobility. In this study, we propose a new theoretical approach to define the rotational diffusion and fluctuating dipole mobility from the experimental loss peak relaxation time. In some recent reports, $^{27, 28}$ we discussed the deconvolution procedure for the BDS data of the imaginary part of $\varepsilon(\omega)$ to obtain the dipolar rotational loss peak frequency, $\omega_d = 2\pi f_d$, and the corresponding rotational relaxation time, $\tau_r = 1/\omega_d$. In general, the relaxation time τ_r is the time needed for the dipole to rotate about 1 rad around the main chain under the applied field E. Therefore, the time $2\pi\tau_r$ corresponds to a full rotation of the fluctuating dipole around the main chain of PVDF. The Stokes-Einstein-Debye hydrodynamic equation relates the relaxation time τ_r to the viscosity η of the surrounding medium (i.e., solvent), 29

$$\tau_r = \frac{\eta \gamma V_{eff}}{k_B T} \tag{7}$$

where γ is a dimensionless prefactor that accounts for the non-spherical shape of the molecule and $V_{\text{eff}} = V_d F(l)$ is the hydrodynamic volume of the molecular dipole. Here, V_d is the true dipole volume, and F(l) is an empirical function that implicitly depends on the slip-stick boundary parameter l. For the stick boundary l=1, $F(l)\approx 1$, and for the slip boundary l=2, 0.1 < F(l) < 0.2. The exact formula for F(l) is currently unknown, but can be empirically derived from experimental results. Rigorously speaking, F(l) for the slip and stick boundary conditions depends on the concentration of dipolar molecules in the solution. For example, in dilute solutions, the difference between F(l=1) and F(l=2) is small.³² For PVDF-like dipolar polymers, F(l) should also include the dipole-dipole interaction parameter. When the dipoles interact strongly with each other, their rotation perpendicular to the main chain slows down, suggesting an increase in F(l). We propose the following formula: $F(l) = \frac{1}{l^3} \frac{n_d}{n_0}$, where n_d and n_0 are the dipole concentrations in the measured and reference systems, respectively. For simplicity, we assume $n_d/n_0 \sim 1$ to concentrate mostly on the *l*-dependence of the dipole mobility. In the dilute dipole case with a stick boundary, F(l=1) = 1. For the slip boundary case, F(l=2) = 1/8, which is consistent with previous reports.²⁹-31

To proceed further theoretically, some simplifying assumptions need to be made. First, we consider the dipole m_d to be a spherical solute (dipole volume V_d) attached to a matrix with a relative permittivity ε_m . Second, we assume that the dipole experiences thermal rotational fluctuations because of its interaction with the matrix. The orientational correlation function [C(t)] for such thermal rotations is generally written as,

$$C(t) = \frac{\langle m_d(0)m_d(t) \rangle}{\langle m_d(0)m_d(0) \rangle}$$
(8)

where the angled brackets indicate the average over equilibrium distribution. The orientational correlation function is usually fitted by a Kohlrausch–Williams–Watt (KWW) function³³⁻³⁵ with the stretching parameter β =1. For interacting dipoles,^{36, 37} this function can be analyzed using a double relaxation time approximation, which contains the one-body (self) and the two-body (pair interaction) parts,

$$C(t) = AC_s(t) + BC_n(t) \tag{9}$$

The self-correlation part $C_s(t)$ describes the rotation of a single dipole in the absence of interaction between particles, whereas the pair correlation part $C_p(t)$ describes the rotation of interacting dipoles. The coefficients A and B are defined from the normalization of C(t). For the system containing N interacting dipoles, $A = N^2/(N^2+N^2/2) = 2/3$ and $B = (N^2/2)/(N^2+N^2/2) = 1/3$. For the self-rotational correlation, we assume exponential decay with relaxation time τ_{r0} , and for the pair interaction rotational correlation the decay has a relaxation time $\tau_r > \tau_{r0}$. For simplicity, it is reasonable to assume a linear dependence of τ_r on the interaction parameter λ ,

$$\tau_r = \tau_{r0}(1+\lambda) \tag{10}$$

The parameter λ represents the strength of the dipole-dipole interaction, and can be expressed in terms of the renormalized orientational susceptibility χ of rotators in space,³⁸

$$\lambda = \frac{\chi}{\varepsilon_0 \varepsilon_m} = \frac{n m_d^2}{3 k_B T \varepsilon_0 \varepsilon_m} \tag{11}$$

where we take into account that $\chi = n \ \alpha_{dip}$, and the orientational polarization of the dipoles $\alpha_{dip} = m_d^2/(3k_BT)$. Eventually, we arrive at,

$$C(t) = \frac{1}{3} \left(2e^{-t/\tau_{r0}} + e^{-t/\tau_r} \right)$$
 (12)

Eqns. (10) and (11) clearly state that the higher the dipole-dipole interaction parameter λ , or, the lower the temperature, the longer the relaxation time τ_r of the dipole, and thus the dielectric loss peak happens at a lower frequency.

Once the relaxation time τ_r (or τ_{r0}) is established, one can proceed to calculate the rotational self-diffusion coefficient D_{r0} for the fluctuating dipole. We use the Einstein relationship for the average mean-square displacement at a rotational angle Ω , 31,39,40

$$\langle \Omega^2(t) \rangle = \ell(\ell+1)D_{r0}t \tag{13}$$

where the boundary parameter is $\ell=1$ for the stick boundary case, where the rotating dipole experiences attractive dipole-solvent and attractive dipole-dipole interactions, and $\ell=2$ for the slip boundary case, where the thermal rotation of the dipole is completely free. Given that,

$$\langle \Omega^2(t = 2\pi \tau_{r_0}) \rangle = 2\pi \tag{14}$$

the following relationship for the rotational diffusion coefficient is obtained,

$$D_{r0} = \frac{1}{\ell(\ell+1)\tau_{r0}} = \frac{1+\lambda}{\ell(\ell+1)\tau_r} \tag{15}$$

Using Eqn. (7), we arrive at,

$$D_{r0} = \frac{1+\lambda}{\ell(\ell+1)F(l)} \frac{k_B T}{\eta \gamma V_d} \tag{16}$$

Several approximations are available for the molecular shape factor γ . In refs. ^{41, 42}, the following γ -factor was used under a stick solute-solvent boundary condition (ℓ =1) for a cylindrical dipole with an aspect ratio $L = b_1/b_2 \ge 1$ (b_1 is the length of the cylinder and b_2 is its diameter),

$$\gamma = \ln(L) - 0.662 + \frac{0.917}{L} - \frac{0.05}{L^2} \tag{17}$$

For a higher aspect ratio L, the shape factor γ increases, which makes the rotational diffusion slower.

Using the theory for charged colloids, the following relation for the concentration dependence of the self-diffusion coefficient can be used, 43, 44

$$D_r(n) = D_{r0}(1 - 0.631\phi - 0.726\phi^2)$$
(18)

where $\phi = nV_d$ is the dipole packing fraction. Finally, we arrive at the general formula for the rotational dipole mobility,

$$\mu_r(n) = \frac{D_r(n)}{k_B T} = \frac{1+\lambda}{\ell(\ell+1)\tau_r} \frac{1}{k_B T} (1 - 0.631\phi - 0.726\phi^2)$$

$$= \frac{l^2}{l+1} \frac{1+\lambda}{\eta \gamma V_d} (1 - 0.631\phi - 0.726\phi^2)$$
(19)

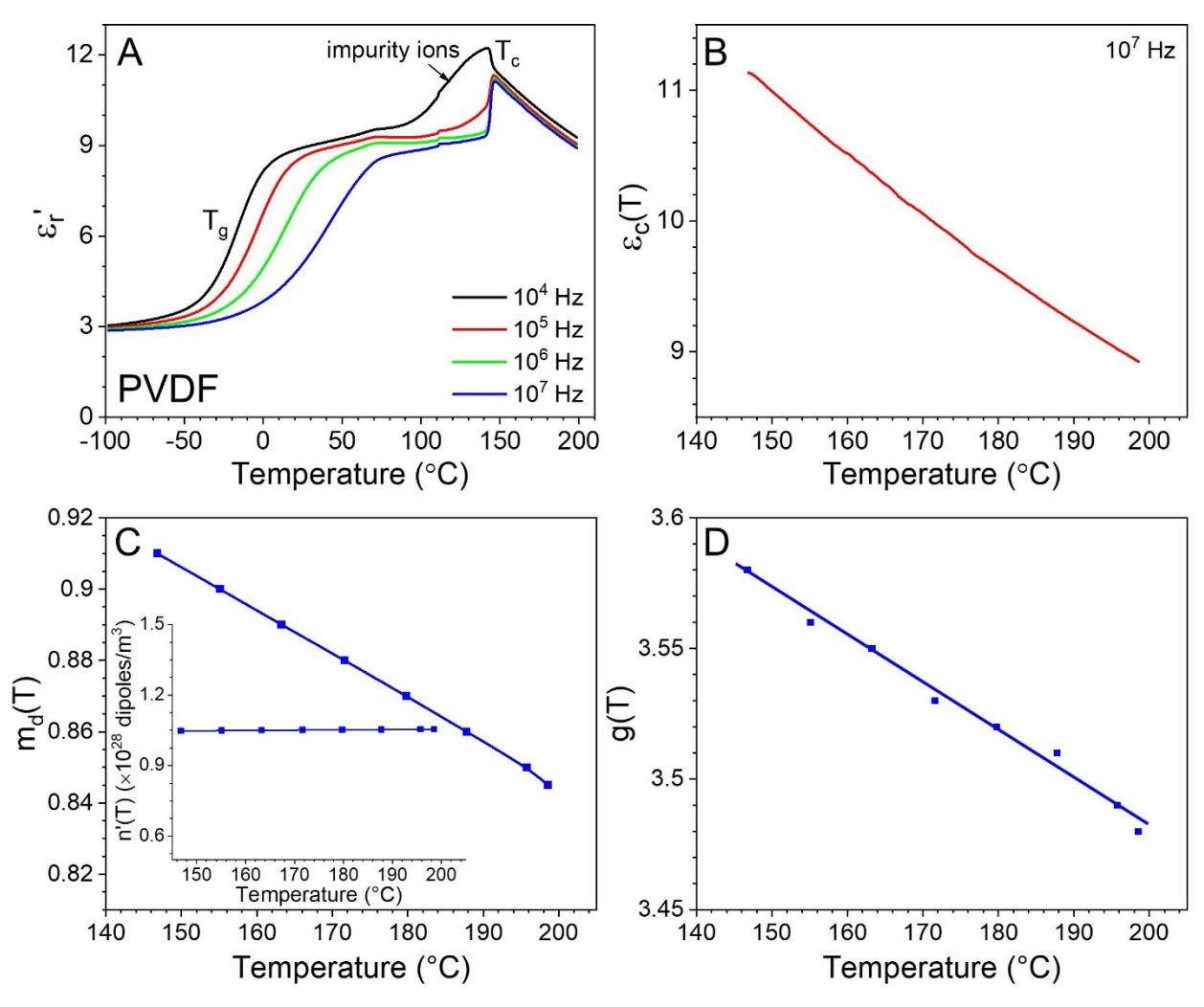


Figure 1. (A) Temperature-scan BDS result of ε_r' at different frequencies and (B) $\varepsilon_c(T)$ as a function of temperature for the melt-recrystallized PVDF. The cooling rate is 2 °C/min. (C) $m_d(T)$ and n'(T), and (D) g(T) as a function of temperature for the molten PVDF.

Molten PVDF with a Constant Dipole Concentration. Figure 1 shows the cooling BDS curves of the real part of the relative permittivity (ϵ_r ') from the melt of PVDF at 200 °C to -100 °C [note that the melting temperature (T_m) of this PVDF was 171 °C^{12, 18}]. Upon cooling, crystals formed at a crystallization temperature (T_c) around 146 °C and the ϵ_r ' exhibited a sudden drop from 11.3 to 9.3 at 10⁷ Hz (Figure 1A). Upon further cooling, the glass transition temperature (T_g) was observed at a lower temperature. We can see that T_g was highly frequency dependent whereas T_c was almost frequency independent. As reported before, ^{27, 28} PVDF was often contaminated with sub-ppm level of impurity ions, whose interfacial polarization was seen to increase the apparent permittivity, especially at high temperatures. From Figure 1A, the ϵ_r ' was not very much affected by impurity ions when the frequency was above 10⁶ Hz. Therefore, the ϵ_r ' of the molten PVDF (i.e., 146 - 200 °C) at 10⁷ Hz was taken as the ϵ_c (T), as presented in Figure 1B.

From the density of molten PVDF (1.680 g/cm³),^{12, 18} the dipole concentration n_0 was found to be $n_0 = 1.58 \times 10^{28} \ m^{-3}$. Because the molten PVDF had a random chain orientation, only 2/3 of n_0 could respond to the applied electric field;¹² therefore, an initial value of $n_0' = 1.05 \times 10^{28} m^{-3}$ was used in the fitting procedure to determine g_0 and m_{d0} , and their coefficients α , β , and θ in Eqns. (3-5). Here, we used $\varepsilon_m = 1$ and $\varepsilon_c^0 = 3$ in Eqn. (2) and allowed n_0' to vary slightly (within 5%) to get the best fit.

For the power law expression used for the dipole moment in Eqn. (5), the following optimal fitting parameters were obtained at $T_0 = 146$ °C: $n_0' = 1.048 \times 10^{28}$ /m³, $m_{d0} = 0.9138$ D, $g_0 = 4.330$, $\alpha = 4.15 \times 10^{-4}$, $\beta = 5.64 \times 10^{-2}$, and $\theta = 0.66$. For the tanh(x) expression used for the dipole moment in Eqn. (6), the following optimal fitting parameters were obtained at $T_0 = 146$ °C: $n_0' = 1.041 \times 10^{28}$ /m³, $m_{d0} = 0.9093$ D, $g_0 = 4.930$, $\alpha = 6.29 \times 10^{-4}$, $\beta = 4.33 \times 10^{-2}$, and $\theta = 0.52$. The temperature dependences of $n_0'(T)$, $m_d(T)$, and g(T) are presented in Figure 1C,D. As we can

see, both $m_d(T)$ and g(T) decreased with increasing temperature, indicating that thermal fluctuation tended to decrease the dipole-dipole interactions for both $m_d(T)$ and g(T). In the following sections, we will use the fitted values of g_0 and α as global parameters for other PVDF samples.

At 140 °C, the *g*-factor of ~2 for water^{12, 23} is significantly smaller than that (~3.59) for PVDF (Figure 1D). This can be attributed to the long-chain connectivity of repeat-unit dipoles, which favors a more or less parallel arrangement of neighboring dipoles in a chain. Note that Eqn. (2) is applicable to three-dimensional freely rotating dipoles, not to long-chain polymers, which have dihedral angle restrictions. Therefore, the orientational dipole polarizability $\alpha_{dip} = m_d^2/(3k_BT)$ is underestimated for PVDF. Consequently, the *g*-factor for PVDF appears to be higher. If we assume that the amorphous phase between two neighboring crystalline lamellae is 100% OAF, the dipolar orientation will be restricted in two dimensions and the dipolar polarizability becomes $\alpha_{dip} = m_d^2/(2k_BT)$. Then, the *g*-factor at 140 °C will be 1.5 times smaller: g = 2.39, which is similar to that of water. For real semicrystalline PVDF with both OAF and isotropic amorphous fraction (IAF) in the amorphous phase, we consider that the *g*-factor should be between 2.39 and 3.59.

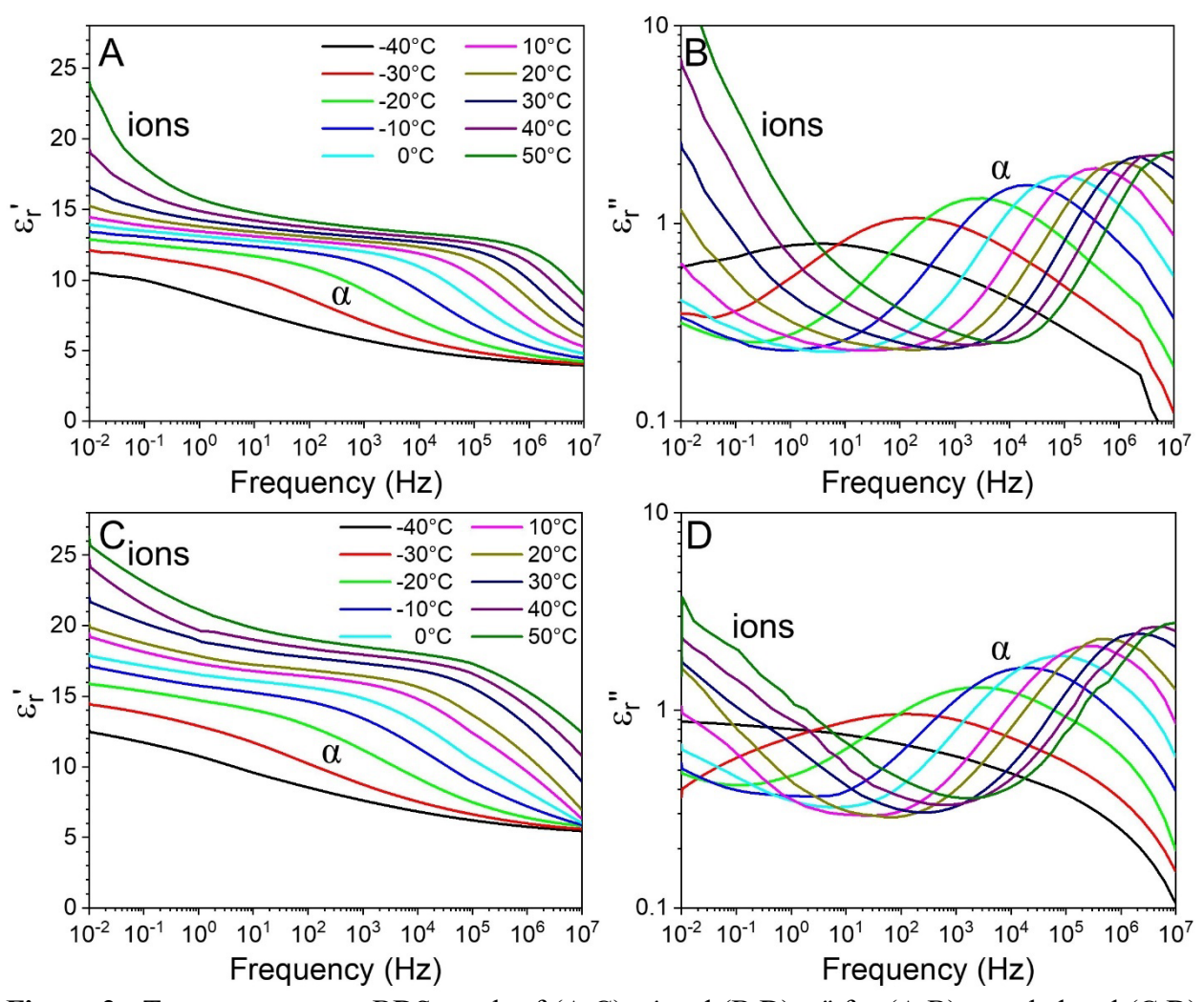


Figure 2. Temperature-scan BDS result of (A,C) ϵ_{r}' and (B,D) ϵ_{r}'' for (A,B) unpoled and (C,D) poled BOPVDF at different frequencies.

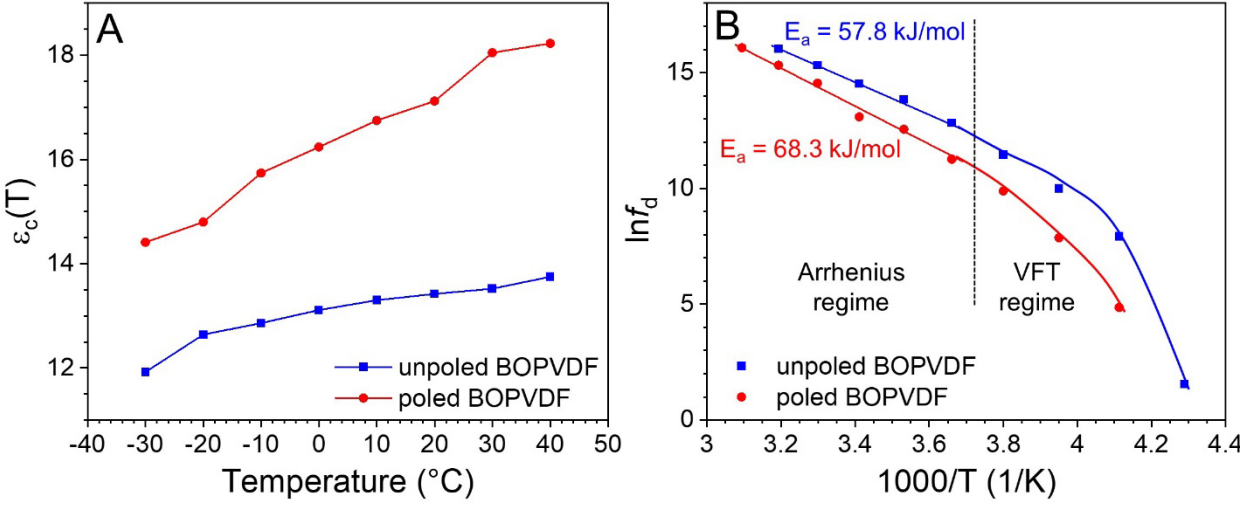
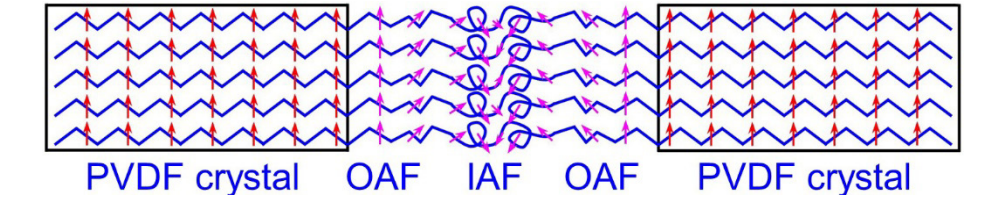


Figure 3. (A) $\epsilon_c(T)$ as a function as temperature (T) and (B) $\ln f_d$ as a function of 1/T for unpoled and poled BOPVDF.

Fitting Experimental $\varepsilon_c(T)$ for Unpoled and Poled BOPVDF Films. To obtain $\varepsilon_c(T)$ data for unpoled and poled BOPVDF films, frequency-scan BDS experiments were performed. Results for ε_r' and ε_r'' (the imaginary part of the relative permittivity) are shown in Figure 2. Step decreases in ε_r' and relaxation peaks in ε_r'' were observed, which belonged to the α transition of amorphous PVDF. The upturns in both ε_r' and ε_r'' at low frequencies and high temperatures were attributed to the interfacial polarization of impurity ions at the polymer/metal electrode interfaces. From the plateau values of ε_r' at low frequencies, $\varepsilon_c(T)$ values were obtained for both unpoled and poled BOPVDF, as plotted in Figure 3A. Both $\varepsilon_c(T)$ values increased with T, and the $\varepsilon_c(T)$ of poled BOPVDF was higher than that of unpoled BOPVDF. From the ε_r'' plots in Figures 2B,D, the logarithmic peak frequency (f_d) was plotted versus 1/T (Figure 3B). Two regimes were observed. At low temperatures (<0 °C), the data fitted the Vogel-Fulcher-Tammann (VFT) equation. ⁴⁵ At high temperatures (>0 °C), the data fitted the Arrhenius equation. From the slopes of fitted Arrhenius equations, the activation energy (ε_a) was obtained: $\varepsilon_a = 57.8 \pm 1.5$ kJ/mol for the unpoled BOPVDF and $\varepsilon_a = 68.3 \pm 3.6$ kJ/mol for the poled BOPVDF.

Scheme 1. Three-Phase Model for BOPVDF with crystal, OAF, and IAF.



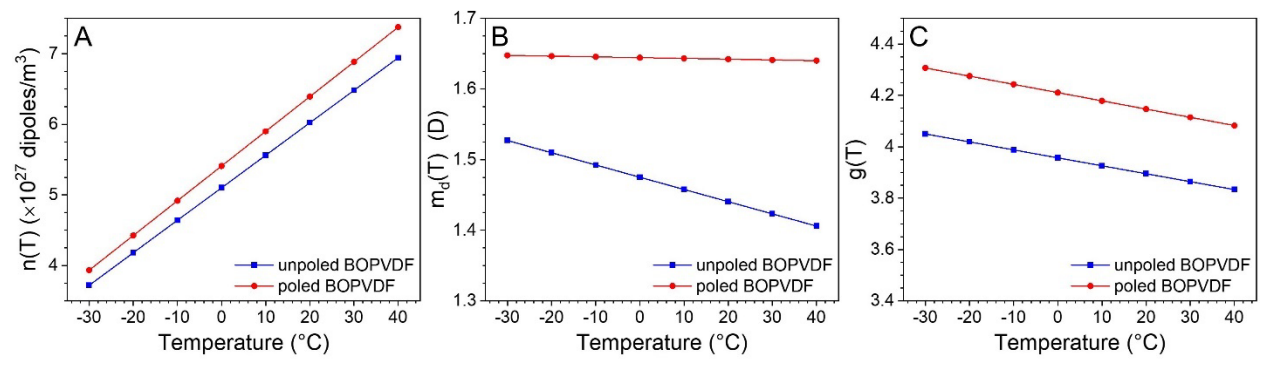


Figure 4. (A) n(T), (B) $m_d(T)$, and (C) g(T) as a function of temperature for unpoled and poled BOPVDF films. The results are obtained using Eqn. (6) for m_d .

Both unpoled and poled BOPVDF had a crystallinity around 0.52.^{12, 18} Under the BDS voltage (i.e., 1 V_{rms}), the crystalline phases should not contribute to the orientational polarization. Taking into account the edge-on orientation of PVDF crystalline lamellae in the film due to biaxial stretching (Scheme 1), the parallel capacitor model is used.¹² Ideally, a three-phase model (i.e., crystal, OAF, and IAF) should be used for the semicrystalline BOPVDF.^{11, 12} However, the Kirkwood-Fröhlich theory could not be applied to the OAF. Therefore, we decided to use the simple two-phase model with crystals and the combined amorphous phase:

$$\varepsilon_c(T) = \varepsilon_{cr}\eta_{cr} + \varepsilon_{am}(T)(1 - \eta_{cr}) \tag{20}$$

where ε_{cr} is the relative permittivity of the PVDF crystals, η_{cr} the packing fraction of the crystals, $\varepsilon_{am}(T)$ the relative permittivity of the combined PVDF amorphous phase. With the values for the crystalline phase: ε_{cr} =3 and η_{cr} =0.52, it was possible to calculate $\varepsilon_{am}(T)$ from Eqn. (20). After fitting, we obtained the following parameters:

i) For the unpoled BOPVDF and with the power law expression used for the dipole moment in Eqn. (5), $n_0 = 2.69 \times 10^{27} \text{ m}^{-3}$, $m_{d0} = 1.44 \text{ D}$, $g_0 = 4.31$, $\alpha = 3.74 \times 10^{-4}$, $\beta = 3.44$, and $\theta = 4.9 \times 10^{-3}$ at $T_0 = -30$ °C. For the unpoled BOPVDF and with the tanh(x) expression used for the dipole moment in Eqn. (6), $n_0 = 3.93 \times 10^{27} \text{ m}^{-3}$, $m_{d0} = 1.53 \text{ D}$, $g_0 = 4.80$, $\alpha = 6.45 \times 10^{-4}$, $\beta = 3.04$, and $\theta = 0.28$ at $T_0 = -30$ °C.

ii) For the poled BOPVDF and with the power law expression used for the dipole moment in Eqn. (5), $n_0 = 3.17 \times 10^{27} \text{ m}^{-3}$, $m_{d0} = 1.53 \text{ D}$, $g_0 = 4.7$, $\alpha = 3.69 \times 10^{-4}$, $\beta = 2.66$, $\theta = 1.91 \times 10^{-4}$ at $T_0 = -30$ °C. For the poled BOPVDF and with the tanh(x) expression used for the dipole moment in Eqn. (6), $n_0 = 3.89 \times 10^{27} \text{ m}^{-3}$, $m_{d0} = 1.65 \text{ D}$, $g_0 = 5.1$, $\alpha = 6.30 \times 10^{-4}$, $\beta = 2.90$, $\theta = 1.58 \times 10^{-2}$ at $T_0 = -30$ °C.

Figure 4A-C shows n(T), $m_d(T)$, and g(T) as a function of T, respectively, when Eqn. (6) is used for m_d . When Eqn. (5) is used for m_d , similar results are obtained; see Figure S1 in the Supporting Information. As temperature increased, n(T) increased linearly [i.e., $\beta > 0$, as seen in Eqn. (3)], which could be explained by the continuous devitrification of the rigid amorphous fraction (RAF) in BOPVDF. 46-48 Note that near T_g , a significant portion of OAF became the RAF, as reported before. 49

The $m_d(T)$ of the poled BOPVDF remained nearly constant around 1.63 D and was higher than that of the unpoled BOPVDF (Figure 4B). Due to the weaker dipole-dipole interactions, $m_d(T)$ of the unpoled BOPVDF gradually decreased with temperature. Note that both m_{d0} values (1.63 D for poled BOPVDF and 1.52 D for unpoled BOPVDF) were significantly higher than that (m_{d0} = 0.91 D) of the molten PVDF. As shown in Figure 4C, g(T) of the poled BOPVDF film was higher than that of the unpoled BOPVDF, and both decreased linearly with increasing temperature. Obviously, the polarized β crystalline lamellae in the poled BOPVDF substantially enhanced the g(T).

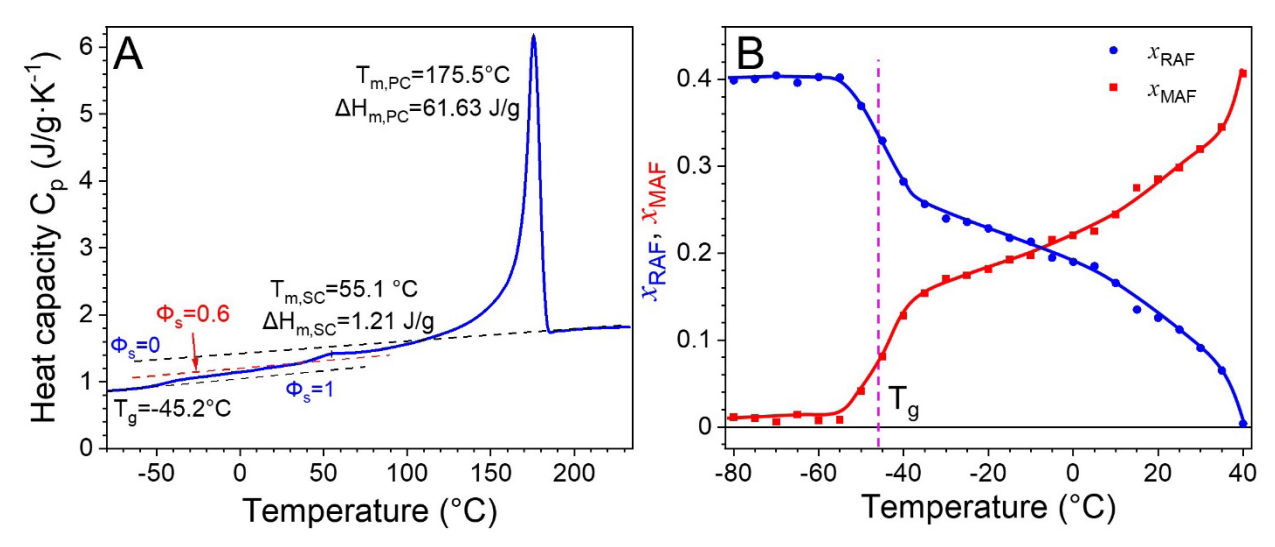


Figure 5. (A) Heating TMDSC curve for the melt-recrystallized BOPVDF at 5 °C/min. The modulation was 0.8 °C at 1 Hz. (B) Calculated x_{RAF} and x_{MAF} as a function of temperature by assuming the crystallinity being 0.59.

To the best of our knowledge, the RAF in α PVDF had only been reported in two publications. First, using ultrafast DSC, Schick and coworkers determined the RAF content around 0.35 at the Tg, assuming a low x_c of 0.25.⁴⁷ Second, Govinna also determined the RAF content for α PVDF to be 0.21-0.28 using conventional TMDSC.⁴⁸ However, no report exists for the devitrification of RAF during heating above Tg. In this work, the devitrification of RAF in PVDF was studied by TMDSC. The heat capacity (Cp) curve of the melt-recrystallized BOPVDF during heating is presented in Figure 5A. The Tg was observed at -45.2 °C. The melting of poor secondary crystals was seen at 55.1 °C with a heat of fusion around 1.21 J/g. The melting of primary crystals was observed at 175.5 °C with a heat of fusion of 61.63 J/g. Because the melt-recrystallized BOPVDF had the α phase, the heat of fusion of perfect α PVDF crystal, Δ H_f° = 104.6 J/g, ⁵⁰ was used to calculate the crystallinity, $x_c = 0.59$. The solid and liquid lines were determined by the linear portion of the Cp curve. Following a previous report and assuming a constant x_c between -80 and 40 °C, the contents of the RAF (x_{RAF}) and mobile amorphous fraction (MAF, x_{MAF}) were determined, and results are shown in Figure 5B. Below -55 °C, x_{RAF} and x_{MAF} were 0.40 and 0.008,

respectively. At T_g (-45.2 °C), x_{RAF} and x_{MAF} were 0.331 and 0.079, respectively. This x_{RAF} of 0.331 at T_g is similar to the value of 0.35 determined by a previous fast DSC study.⁴⁷ At the end of the glass transition (-30 °C), x_{RAF} and x_{MAF} were 0.244 and 0.166, respectively. Upon further increase the temperature, x_{RAF} continuously decreased and x_{MAF} gradually increased. This was direct evidence of RAF devitrification upon heating. Finally, at 40 °C, x_{RAF} decreased to 0.014 and x_{MAF} increased to 0.396. From this work, devitrification of RAF took place (around -10 °C) before the observable onset of secondary crystal melting (around 30 °C), similar to a previous report for PET.⁵¹ Following the melting of secondary crystals (at 55.1 °C), the primary crystals started to melt around 80 °C. The low onset crystal melting temperature for PVDF was believed to be a result of the head-head and tail-tail defects (usually ~5 mol.%) in radically polymerized PVDF. Note that RAF and MAF are different from OAF and IAF, as discussed previously,⁴⁹ and their contents are different. This is because RAF/MAF are defined by chain mobility whereas OAF/IAF are defined from the semicrystalline structure.

Using the x_{RAF} and x_{MAF} values in Figure 5B, we could extract the dielectric constants of the devitrified OAF (i.e., mobile OAF or MOAF) by assuming a parallel capacitor model. The derivation and results are shown in Section S2 of the Supporting Information. As we can see from Figure S2, the dielectric constant of MOAF was higher for the poled BOPVDF than the unpoled BOPVDF. This could be attributed to the enhanced local electric field from the highly polarized β PVDF crystals, as reported before. Although the dielectric constants of the MOAF could be obtained, the Kirkwood-Fröhlich theory could not be applied to the MOAF. Therefore, we could not use Eqn. (2) to extract the information of n(T), $m_d(T)$, and g(T) for the MOAF. Instead, we should consider OAF and IAF as a whole and use Eqn. (20) to obtain the $\varepsilon_{am}(T)$. As a result, the

 $\varepsilon_{am}(T)$ and the g(T) were overestimated. This is the reason why the g(T) values for both unpoled and poled BOPVDF were higher than those of water (g = 2.4) and methanol (g = 2.7) at 0 °C.

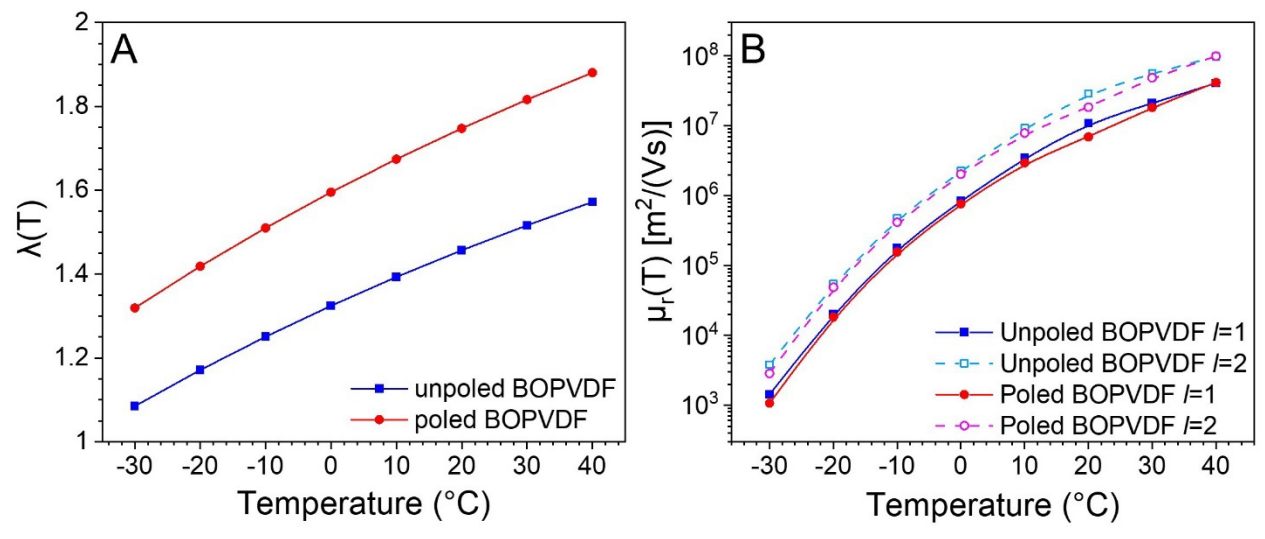


Figure 6. (A) Dipole-dipole interaction strength parameter $\lambda(T)$ and (B) rotational dipole mobility $\mu_r(T)$ for the unpoled and poled BOPVDF under stick (l=1) and slip (l=2) boundary conditions. The results are obtained using Eqn. (6) for m_d .

Using Eqn. (6) for m_d , the dipole-dipole interaction strength parameter $\lambda(T)$ and the rotational dipole mobility $\mu_r(T)$ were obtained; see Figure 6. When Eqn. (5) was used for m_d , similar results of $\lambda(T)$ and $\mu_r(T)$ are shown in Figure S3 of the Supporting information. In Figure 6A, with T. In Eqn. (11), λ had an explicit 1/T dependence and implicit dependence on T through the dipole concentration n and the dipole moment m_d . Also, λ was higher for the poled BOPVDF compared with that for the unpoled BOPVDF. Meanwhile, the calculated rotational dipole mobility for the poled BOPVDF was about 1.2 times that of the unpoled BOPVDF, regardless of the stick or slip condition (Figure 6B). This could be a result of the higher m_d for the poled BOPVDF. Interestingly, the increase of μ_r was over 4 orders of magnitude from -30 to 40 °C with a steeper slope below 0 °C. Such a large increase in the rotational dipole mobility directly reflected the significant devitrification of RAF in PVDF (see Figure 5), and can be attributed to the increased

dipole-dipole interaction strength λ (see Figure 6A). This devitrification of RAF in PVDF upon heating appeared to be much easier than that in nonpolar and weakly polar polymers, such as isotactic polystyrene, poly(butylene terephthalate), and poly(ethylene terephthalate) (PET), reported in the literature. We consider that the large dipole moment and strong dipole-dipole interaction should be responsible for the easier devitrification of RAF in PVDF. Consequently, the permittivity of PVDF did not decrease for $T > T_g$ (see Figure 1A), which is different from the case observed in weakly polar polymers such as PET. Meanwhile, we consider that the stick boundary condition, rather than the slip boundary condition, should apply for PVDF in the solid-state because of the strong dipole-dipole interactions. We note that the high dipole mobility at room temperature also accounts for the enhanced electrostrictive and piezoelectric 11, 13, 14 properties for PVDF and P(VDF-TrFE)-based random copolymers and terpolymers.

Conclusions

In addition to the pronounced ferroelectric contribution from its crystalline phase (especially the β phase), PVDF also exhibits a high static permittivity (ε_c = 9-15) at low electric fields (well below the coercive field). This is attributed to the mobile dipoles in the amorphous PVDF, which have relatively large dipole moments per repeat unit. To investigate the origin of the higher permittivity of the poled BOPVDF relative to that of the unpoled BOPVDF,^{12, 18} we carried out a combined BDS and theoretical study of the rotational dipole mobility within the framework of a crystalline-amorphous two-phase model. From the BDS data of the molten PVDF, the *g*-factor and its temperature dependence α were first determined using Kirkwood-Fröhlich theory, and these were then used as the global parameters to fit the experimental BDS data of unpoled and poled BOPVDF. Subsequently, their n(T), $m_d(T)$, and g(T) values were deduced. As the temperature

increased from -30 to 40 °C, the active dipole concentration n(T) significantly increased from 3×10^{27} to 5.5×10^{27} dipoles/m³, which suggested the devitrification of the RAF in PVDF with increasing temperature. While the n(T) values were similar for unpoled and poled BOPVDF, the $m_d(T)$ and g(T) of poled BOPVDF were higher than those of unpoled BOPVDF. This could be attributed to the enhanced local electric field due to highly polarized β crystals in the poled BOPVDF.

Using the theory of charged particles, we developed a new theory to estimate the rotational dipole mobility for polar polymers. As a result of the increased n(T) and large dipole moment m_d of both unpoled and poled BOPVDF, the dipole-dipole interaction parameter λ was found to increase with increasing temperature. It is the large dipole moment and increased dipole-dipole interaction that caused the substantial increase in rotational dipole mobility, i.e., over 4 orders of magnitude from -30 to 40 °C, for PVDF. Again, this directly indicated the easy devitrification of RAF in PVDF upon heating.

Acknowledgments

L.Z. and P.L.T. acknowledge financial support from National Science Foundation, Division of Materials Research, Polymers Program (DMR-2103196). E.A. acknowledges the financial support from the Ministry of Science and Higher Education of the Russian Federation (State Assignment No. 075-01056-22-00). We thank Prof. Peggy Cebe at Tufts University for the helpful discussion of TMDSC measurements.

Conflict of Interest

The authors declare no conflict of interest.

References

- 1. Zhu, L. Exploring Strategies for High Dielectric Constant and Low Loss Polymer Dielectrics. *J. Phys. Chem. Lett.* **2014,** *5,* 3677-3687.
- 2. Wei, J.; Zhu, L. Intrinsic Polymer Dielectrics for High Energy Density and Low Loss Electric Energy Storage. *Prog. Polym. Sci.* **2020**, *106*, 101254.
- 3. Wu, X; Chen, X.; Zhang, Q. M.; Tan, D. Q. Advanced Dielectric Polymers for Energy Storage. *Energy Storage Mater.* **2022**, *44*, 29-47.
- Feng, Q.-K.; Zhong, S.-L.; Pei, J.-Y.; Zhao, Y.; Zhang, D.-L.; Liu, D.-F.; Zhang, Y.-X.;
 Dang, Z.-M. Recent Progress and Future Prospects on All-Organic Polymer Dielectrics for
 Energy Storage Capacitors. *Chem. Rev.* 2022, 122, 3820-3878.
- 5. Li, H.; Zhou, Y.; Liu, Y.; Liu, Y.; Wang, Q. Dielectric Polymers for High-Temperature Capacitive Energy Storage. *Chem. Soc. Rev.* **2021**, *50*, 6369-6400.
- Luo, H.; Zhou, X.; Ellingford, C.; Zhang, Y.; Chen, S.; Zhou, K.; Zhang, D.; Bowen, C.
 R.; Wan, C. Interface Design for High Energy Density Polymer Nanocomposites. *Chem. Soc. Rev.* 2019, 48, 4424-4465.
- 7. Elton, D. C.; Fernandez-Serra, M. V. Polar Nanoregions in Water: A Study of the Dielectric Properties of TIP4P/2005, TIP4P/2005f and TTM3F. *J. Chem. Phys.* **2014**, *140*, 124504.
- 8. Fukasawa, T.; Sato, T.; Watanabe, J.; Hama, Y.; Kunz, W.; Buchner, R. Relation Between Dielectric and Low-Frequency Raman Spectra of Hydrogen-Bond Liquids. *Phys. Rev. Lett.* **2005,** *95*, 197802.
- 9. Buchner, R.; Hefter, G. Interactions and Dynamics in Electrolyte Solutions by Dielectric Spectroscopy. *Phys. Chem. Chem. Phys.* **2009**, *11*, 8984-8999.

- 10. Artemov, V. G.; Volkov, A. A. Water and Ice Dielectric Spectra Scaling at 0°C. Ferroelectrics 2014, 466, 158-165.
- 11. Huang, Y.; Rui, G.; Li, Q.; Allahyarov, E.; Li, R.; Fukuto, M.; Zhong, G.; Xu, J; Li, Z.; Taylor, P. L.; Zhu, L. Enhanced Piezoelectricity from Highly Polarizable Oriented Amorphous Fractions in Biaxially Oriented Poly(vinylidene fluoride) with Pure β Crystals. Nat. Commun. 2021, 12, 675.
- 12. Rui, G.; Huang, Y.; Chen, X.; Li, R.; Wang, D.; Miyoshi, T.; Zhu, L. Giant Spontaneous Polarization for Enhanced Ferroelectric Properties of Biaxially Oriented Poly(vinylidene fluoride) by Mobile Oriented Amorphous Fractions. *J. Mater. Chem. C* **2021**, *9*, 894-907.
- 13. Zhu, Z.; Rui, G.; Li, Q.; Allahyarov, E.; Li, R.; Soulestin, T.; Domingues Dos Santos, F.; He, H.; Taylor, P.; Zhu, L. Electrostriction-Enhanced Giant Piezoelectricity via Relaxor-Like Secondary Crystals in Extended-Chain Ferroelectric Polymers. *Matter* 2021, 4, 3696-3709.
- 14. Zhu, Z.; Rui, G.; Li, R.; He, H.; Zhu, L. Effect of Dipole Mobility in Secondary Crystals on Piezoelectricity of a Poly(vinylidene fluoride-co-trifluoroethylene) 52/48 mol % Random Copolymer with An Extended-Chain Crystal Structure. Macromolecules 2021, 54, 9879-9887.
- 15. Rui, G.; Allahyarov, E.; Li, R.; Taylor, P. L.; Zhu, L. Hard-to-Soft Transition-Enhanced Piezoelectricity in Poly(vinylidene fluoride) via Relaxor-Like Secondary Crystals Activated by High-Power Ultrasonication. *Mater. Horizons* **2022**, *9*, 1992-1998.
- Liu, Y.; Aziguli, H.; Zhang, B.; Xu, W. H.; Lu, W.; Bernholc, J.; Wang, Q. Ferroelectric Polymers Exhibiting Behaviour Reminiscent of a Morphotropic Phase Boundary. *Nature* 2018, 562, 96-100.

- 17. Liu, Y.; Wang, Q. Ferroelectric Polymers Exhibiting Negative Longitudinal Piezoelectric Coefficient: Progress and Prospects. *Adv. Sci.* **2020,** *7,* 1902468.
- 18. Yang, L.; Ho, J.; Allahyarov, E.; Mu, R.; Zhu, L. Semicrystalline Structure Dielectric Property Relationship and Electrical Conduction in a Biaxially Oriented Poly(vinylidene fluoride) Film Under High Electric Fields and High Temperatures. *ACS Appl. Mater. Interfaces* **2015**, *7*, 19894-19905.
- 19. Kao, K., Dielectric Phenomena in Solids: with Emphasis on Physical Concepts of Electronic Processes; Elsevier Academic Press: Boston, 2004.
- 20. Dejardin, P. M.; Pabst, F.; Cornaton, Y.; Helbling, A.; Blochowicz, T. Temperature Dependence of the Kirkwood Correlation Factor and Linear Dielectric Constant of Simple Isotropic Polar Fluids. *Phys. Rev. E* 2022, *105*, 024108.
- 21. Dejardin, P. M. Kinetic Yvon-Born-Green Theory of the Linear Dielectric Constant and Complex Permittivity of Isotropic Polar Fluids. *Phys. Rev. E* **2022**, *105*, 024109.
- Wertheim, M. S. Theory of Polar Fluids. IV. Fluctuations and Inequalities. *Mol. Phys.* 1978, 36, 1217-1240.
- 23. Elton, D. C. Understanding the Dielectric Properties of Water. Stony Brook University,2016.
- 24. Maribo-Mogensen, B.; Kontogeorgis, G. M.; Thomsen, K. Modeling of Dielectric Properties of Complex Fluids with an Equation of State. *J. Phys. Chem. B* 2013, 117, 3389-3397.
- Hodge, I. M.; Angell, C. A. Relative Permittivity of Supercooled Water. J. Chem. Phys.
 1978, 68, 1363-1368.

- Fernandez, D. P.; Goodwin, A. R. H.; Lemmon, E. W.; Sengers, J. M. H. L.; Williams, R. C. A Formulation for the Static Permittivity of Water and Steam at Temperatures from 238 K to 873 K at Pressures up to 1200 MPa, Including Derivatives and Debye-Huckel Coefficients. J. Phys. Chem. Ref. Data 1997, 26, 1125-1166.
- 27. Chen, X.; Allahyarov, E.; Li, Q.; Langhe, D.; Ponting, M.; Schuele, D.; Baer, E.; Zhu, L. Reducing Dielectric Loss by Nanoconfined Impurity Ion Transport in Multilayer Films Under Low Electric Fields. *Compos. B: Eng.* 2020, 190, 107908.
- 28. Chen, X.; Allahyarov, E.; Langhe, D.; Ponting, M.; Li, R.; Fukuto, M.; Schuele, D.; Baer, E.; Zhu, L. Reducing Dielectric Loss and Enhancing Electrical Insulation for Multilayer Polymer Films by Nanoconfined Ion Transport Under High Poling Electric Fields. J. Mater. Chem. C 2020, 8, 6102-6117.
- Inamdar, S. R., Rotational Dynamics of Nonpolar and Dipolar Molecules in Polar and Binary Solvent Mixtures. In Hydrodynamics, Schulz, H. E., Simões, A. L. A., Lobosco, R. J., Ed. IntechOpen: London, 2011, Chapter 9, pp. 185-226.
- 30. Nicholas, A. M. de P.; Wasylishen, R. E. Rotations of Linear Triatomic Anions in Aqueous Solution by Nuclear Magnetic Resonance Spectroscopy. *Can. J. Chem.* **1986**, *64*, 1839-1844.
- 31. Huang, M.-M.; Bulut, S.; Krossing, I.; Weingärtner, H. Communication: Are Hydrodynamic Models Suited for Describing the Reorientational Dynamics of Ions in Ionic Liquids? A Case Study of Methylimidazolium Tetra(hexafluoroisopropoxy)aluminates. *J. Chem. Phys.* **2010**, *133*, 101101.

- 32. Sturlaugson, A. L.; Fruchey, K. S.; Lynch, S. R.; Aragón, S. R.; Fayer, M. D. Orientational and Translational Dynamics of Polyether/Water Solutions. *J. Phys. Chem. B* **2010**, *114*, 5350-5358.
- 33. Deschenes, L. A.; Vanden Bout, D. A. Heterogeneous Dynamics and Domains in Supercooled *o*-Terphenyl: A Single Molecule Study. *J. Phys. Chem. B* **2002**, *106*, 11438-11445.
- 34. Tomczak, N.; Vallée, R. A. L.; van Dijk, E. M. H. P.; García-Parajó, M.; Kuipers, L.; van Hulst, N. F.; Julius Vancso, G. Probing Polymers with Single Fluorescent Molecules. Eur. Polym. J. 2004, 40, 1001-1011.
- 35. Schob, A.; Cichos, F.; Schuster, J.; von Borczyskowski, C. Reorientation and Translation of Individual Dye Molecules in a Polymer Matrix. *Eur. Polym. J.* **2004**, *40*, 1019-1026.
- 36. Jones, R. B. Rotational Diffusion of a Tracer Colloid Particle. 2. Long-Time Orientational Correlations. *Physica A* **1989**, *157*, 752-768.
- 37. Alavi, F. N.; Jones, R. B. Rotational Diffusion of a Tracer Colloid Particle. 3. Weak External-Field Effects. *Physica A* **1990**, *165*, 170-195.
- 38. Coffey, W. T.; Kalmykov, Y. P.; Titov, S. V. Fractional Rotational Diffusion and Anomalous Dielectric Relaxation in Dipole Systems. In *Fractals, Diffusion, and Relaxation in Disordered Complex Systems Advances in Physical Chemistry, Part B*, Coffey, W. T., Kalmykov, Y. P., Eds.; Wiley: New York, 2006, 133, 285-437.
- Dote, J.; Kivelson, D.; Schwartz, R. N. A Molecular Quasi-Hydrodynamic Free-Space Model for Molecular Rotational Relaxation in Liquids. *J. Phys. Chem.* 1981, 85, 2169-2180.

- 40. Ivanov, E. N. Theory of Rotational Brownian Motion. Sov. Phys.-JETP 1964, 18, 1041-1045.
- 41. Kharazmi, A.; Priezjev, N. V. Molecular Dynamics Simulations of the Rotational and Translational Diffusion of a Janus Rod-Shaped Nanoparticle. *J. Phys. Chem. B* **2017**, *121*, 7133-7139.
- 42. Tirado, M. M.; Martinez, C. L.; Delatorre, J. G. Comparison of Theories for the Translational and Rotational Diffusion-Coefficients of Rod-Like Macromolecules Application to Short DNA Fragments. *J. Chem. Phys.* **1984**, *81*, 2047-2052.
- 43. Makuch, K.; Heinen, M.; Abade, G. C.; Nägeled, G. Rotational Self-Diffusion in Suspensions of Charged Particles: Simulations and Revised Beenakker-Mazur and Pairwise Additivity Methods. *Soft Matter* **2015**, *11*, 5313-5326.
- Cichocki, B.; Ekiel-Jeżewska, M. L.; Wajnryb, E. Lubrication Corrections for Three-Particle Contribution to Short-Time Self-Diffusion Coefficients in Colloidal Dispersions.
 J. Chem. Phys. 1999, 111, 3265-3273.
- 45. Garciacolin, L. S.; Delcastillo, L. F.; Goldstein, P. Theoretical Basis for the Vogel-Fulcher-Tammann Equation. *Phys. Rev. B* **1989**, *40*, 7040-7044.
- 46. Wunderlich, B. Reversible Crystallization and the Rigid-Amorphous Phase in Demicrystalline Macromolecules. *Prog. Polym. Sci.* **2003**, *28*, 383-450.
- 47. Gradys, A.; Sajkiewicz, P.; Adamovsky, S.; Minakov, A.; Schick, C. Crystallization of Poly(vinylidene fluoride) During Ultra-Fast Cooling. *Thermochim. Acta* **2007**, *461*, 153-157.
- 48. Govinna, N. D. Fundamental and Applied Investigations of Poly(vinylidene fluoride)
 Blends for Filtration Applications. Tufts University, Cambridge, MA, 2019.

- 49. Fu, Y. G.; Busing, W. R.; Jin, Y. M.; Affholter, K. A.; Wunderlich, B. Structure-Analysis of the Noncrystalline Material in Poly(Ethylene-Terephthalate) Fibers. *Macromol. Chem. Phys.* **1994**, *195*, 803-822.
- 50. Nakagawa, K.; Ishida, Y. Annealing Effects in Poly(vinylidene fluoride) as Revealed by Specific Volume Measurements, Differential Scanning Calorimetry, and Electron Microscopy. *J. Polym. Sci., Part B: Polym. Phys.* **1973**, *11*, 2153-2171.
- 51. Chen, H.; Cebe, P. Vitrification and Devitrification of Rigid Amorphous Fraction of PET during Quasi-Isothermal Cooling and Heating. *Macromolecules* **2009**, *42*, 288-292.
- 52. Righetti, M. C.; Di Lorenzo, M. L. Rigid Amorphous Fraction and Multiple Melting Behavior in Poly(butylene terephthalate) and Isotactic Polystyrene. *J. Therm. Anal. Calorim.* **2016**, *126*, 521-530.
- 53. Righetti, M. C.; Laus, M.; Di Lorenzo, M. L. Temperature Dependence of the Rigid Amorphous Fraction in Poly(ethylene terephthalate). *Eur. Polym. J.* **2014**, *58*, 60-68.
- 54. Li, Y.; Makita, Y.; Zhang, G.; Rui, G.; Li, Z.; Zhong, G.; Miyoshi, T.; Huang, H.; Zhu, L. Effects of Rigid Amorphous Fraction and Lamellar Crystal Orientation on Electrical Insulation of Poly(ethylene terephthalate) Films. *Macromolecules* 2020, 53, 3967-3977.
- 55. Wongwirat, T.; Zhu, Z.; Rui, G.; Li, R.; Laoratanakul, P.; He, H.; Manuspiya, H.; Zhu, L. Origins of Electrostriction in Poly(vinylidene fluoride)-Based Ferroelectric Polymers.
 Macromolecules 2020, 53, 10942-10954.